SCIENCE CHINA Materials ARTICLES

mater.scichina.com link.springer.com

Published online 5 March 2020 | https://doi.org/10.1007/s40843-020-1267-2
Sci China Mater 2020, 63(6): 949–958

SPECIAL TOPIC: Single-atom Catalysts

High-loading and thermally stable $Pt_1/MgAl_{1.2}Fe_{0.8}O_4$ single-atom catalysts for high-temperature applications

Kaipeng Liu[1,2†], Yan Tang[3†], Zhiyang Yu[4], Binghui Ge[5], Guoqing Ren[1,2], Yujing Ren[1,2], Yang Su[1], Jingcai Zhang[1], Xiucheng Sun[1,2], Zhiqiang Chen[1], Xiaoyan Liu[1], Botao Qiao[1*], Wei-Zhen Li[1*], Aiqin Wang[1] and Jun Li[3,6*]

ABSTRACT **Single-atom catalysts (SACs) have attracted extensive attention in the field of heterogeneous catalysis. However, the fabrication of SACs with high loading and high-temperature stability remains a grand challenge, especially on oxide supports. In this work, we have demonstrated that through strong covalent metal-support interaction, high-loading and thermally stable single-atom Pt catalysts can be readily prepared by using Fe modified spinel as support. Better catalytic performance in N_2O decomposition reaction is obtained on such SACs than their nanocatalyst counterpart and low-surface-area Fe_2O_3 supported Pt SACs. This work provides a strategy for the fabrication of high-loading and thermally stable SACs for applications at high temperatures.**

Keywords: high loading, thermal stability, single-atom catalyst, strong covalent metal-support interaction, N_2O decomposition

INTRODUCTION

Single-atom catalysts (SACs) have emerged as a new frontier in heterogeneous catalysis due to their maximized atomic efficiency, homogenously dispersed active sites and the potential to bridge homo- and heterogeneous catalysis, among others [1–7]. SACs have demonstrated superior catalytic performance (activity and/or selectivity) in a wide variety of important industrial reactions including oxidation or selective oxidation [1,8–10], hydrogenation or selective hydrogenation [7,11–13], electrochemical catalysis [14–16] and photo-catalysis reactions [17,18]. However, despite the great interests in fundamental study and potential in practical applications, the development of thermally stable SACs, especially with high metal loading remains a grand challenge because the highly dispersed single atoms are often thermodynamically unstable, thus prone to sinter to decrease their surface energy [19,20].

This issue has been partially addressed by the fabrication of various carbon or N-doped carbon supported SACs, where M-C and M-N (M = metal atoms such as Pt, Pd, Ru, Fe, Co, Ni) covalent bonding exist [21–23]. However, currently the applications of these catalysts are mainly limited in electrochemical catalysis on account of their carbon material supports [24,25]. On the other hand, CeO_2 supported Pt SACs prepared by an atomic trapping method are promising for the synthesis of thermally stable oxide-supported SACs [9,19], although the universality of this method needs further determination.

Recently we discovered that single Au atoms can be

[1] CAS Key Laboratory of Science and Technology on Applied Catalysis, Dalian Institute of Chemical Physics, Chinese Academy of Sciences, Dalian 116023, China
[2] University of Chinese Academy of Sciences, Beijing 100049, China
[3] Department of Chemistry & Key Laboratory of Organic Optoelectronics and Molecular Engineering of the Ministry of Education, Tsinghua University, Beijing 100084, China
[4] State Key Laboratory of Photocatalysis on Energy and Environment, College of Chemistry, Fuzhou University, Fuzhou 350002, China
[5] Institute of Physical Science and Information Technology, Anhui University, Hefei 230601, China
[6] Department of Chemistry, Southern University of Science and Technology, Shenzhen 518055, China
[†] These authors contributed equally to this work.
[*] Corresponding authors (emails: bqiao@dicp.ac.cn (Qiao B); weizhenli@dicp.ac.cn (Li W); junli@tsinghua.edu.cn (Li J))

stabilized on oxide supports through a strong covalent metal-support interaction (CMSI) [26,27]. Later on we further found that Pt nanoparticles (NPs) supported on iron oxides could be dispersed into single atoms upon high-temperature calcination [28]. It turns out that a strong CMSI between Fe and Pt is critical to the dispersion process because a Fe-doped Al_2O_3 can stabilize the Pt single atoms as well whereas the undoped one cannot. We hence believe this tactic could be used as a general strategy to synthesize thermally stable SACs, which, however, remains to be exclusively demonstrated.

Herein we report the synthesis of thermally stable Pt SACs according to this strategy by using Fe-modified $MgAl_2O_4$ spinel ($MgAl_{1.2}Fe_{0.8}O_4$, designed as MAFO) as support. Spinels, mixed metal oxides with well-defined structures and excellent thermal stability, are ideal supports for the fabrication of thermally stable catalysts [29,30] due to their capability in stabilizing noble metals at high temperatures and their large specific surface area that can be used to facilitate the preparation of high-loading SACs [30]. Introduction of Fe is expected to stabilize Pt single atoms through strong CMSI. Pt NPs/clusters deposited on MAFO are dispersed into single atoms upon high-temperature calcination. Detailed experimental characterizations together with density functional theory (DFT) calculation reveal that the introduction of Fe plays a critical role in stabilizing the Pt single atoms through a strong interaction between Pt and FeO_x species. Pt_1/MAFO SACs with Pt loading of as high as 5 wt% can be obtained by using this method and show superior catalytic performance in N_2O decomposition compared with its nanocatalyst counterpart and Pt_1/Fe_2O_3 SACs.

EXPERIMENTAL SECTION

Reagents

Magnesium nitrate hexahydrate, magnesium acetate tetrahydrate, iron(III) nitrate nonahydrate were purchased from Tianjin Damao. Aluminum isopropoxide, iron(III) acetylacetonate were bought from Aladdin. Ethanol, NaOH and ethylene glycol were purchased from Tianjin Kemiou. $H_2PtCl_6{\cdot}6H_2O$ was commercially provided by Tianjin Fengchuan. Ultrapure water was obtained from a Millipore Autopure system. All reagents were used without further purification.

Catalysts preparation

Preparation of $MgAl_{1.2}Fe_{0.8}O_4$ spinel

$MgAl_{1.2}Fe_{0.8}O_4$ spinel was prepared by hydrolysis of aluminum isopropoxide, iron(III) acetylacetonate with magnesium nitrate hexahydrate in ethanol. Magnesium nitrate hexahydrate (0.15 mol), aluminum isopropoxide (0.18 mol) and iron(III) acetylacetonate (0.12 mol) were mixed in 900 mL of ethanol and sealed in a 2-L autoclave. The mixture was heated to 120°C and held for 10 h, then increased to 160°C and held for another 10 h under vigorous stirring. After cooling to room temperature, the obtained product was filtrated and then dried at 120°C for 1 h, and finally calcined in ambient air at 700°C for 5 h with a heating rate of 2°C/min. The $MgAl_{1.2}Fe_{0.8}O_4$ spinel is designated as MAFO.

Preparation of $MgAl_2O_4$ spinel

$MgAl_2O_4$ spinel was prepared by hydrolysis of aluminum isopropoxide and magnesium acetate tetrahydrate in ethanol. Magnesium acetate tetrahydrate (0.15 mol) and aluminum isopropoxide (0.30 mol) were mixed in 900 mL of ethanol and sealed in a 2-L autoclave. The mixture was heated to 120°C and held for 10 h, then increased to 160°C and held for another 10 h under vigorous stirring. After cooling to room temperature, the obtained product was filtrated and then dried at 120°C for 1 h, and finally calcined in ambient air at 700°C for 5 h with a heating rate of 2°C/min.

Preparation of Pt/MAFO-CD samples

The Pt/MAFO-CD samples were prepared using the colloid deposition (CD) method. The Pt colloidal solution was synthesized according to the literature [31]. Typically, a solution of NaOH in ethylene glycol (EG) (50 mL, 0.5 mol L^{-1}) and a solution of $H_2PtCl_6{\cdot}6H_2O$ in EG (50 mL, 20 mg mL^{-1}) were mixed together and stirred at room temperature for 30 min under Ar atmosphere. The resulting Pt colloidal solution (Pt: 3.7 mg mL^{-1}) was obtained by heating the solution at 160°C for 3 h under Ar atmosphere. Next, 2 g of MAFO spinel was dispersed into 200 mL of EG solution and the suspension was stirred at 80°C for 30 min. The Pt colloidal solution was added dropwise to the suspension with nominal weight loadings of 1.0 and 3.2 wt%. After being stirred for 3 h and aged for 1 h, the suspensions were then filtrated and washed with 1 L of hot ultrapure water. The filter cake was dried at 60°C overnight and then calcined in ambient air at different temperatures for various time with a heating rate of 2°C/min. The resulting samples are designated as *x*Pt/MAFO-CD-*T*-*t*, where "*x*" is nominal weight loading of Pt, "*T*" is calcination temperature and "*t*" is calcination time. For simplicity, the 1Pt/MAFO-CD-*T*-5h samples are marked as Pt-CD-*T* and the 3.2Pt/MAFO-CD-700-

144h sample (the actual weight loading of Pt measured by inductively coupled plasma optical emission spectrometry (ICP-OES) is 3.1 wt%, shown in Table S1) is marked as 3Pt-CD-700.

Preparation of Pt/MAFO-IWI samples

The Pt/MAFO-IWI samples were prepared by the incipient wetness impregnation (IWI) method. Briefly, an appropriate amount of H_2PtCl_6 solution was added to 2 g of MAFO spinel with nominal weight loading of 1.0, 3.5, 4.0, 4.5 and 5.1 wt%. The mixture was dried at room temperature for 24 h and 60°C overnight. Then, the mixture was calcined in ambient air at different temperatures for different time with a heating rate of 2°C/min. The resulting samples are designated as *x*Pt/MAFO-IWI-*T*-*t*, where "*x*" is nominal weight loading of Pt, "*T*" is calcination temperature and "*t*" is calcination time. For simplicity, the 5.1Pt/MAFO-IWI-720-72h sample (the actual weight loading of Pt measured by ICP-OES is 5.0 wt%, shown in Table S1) is marked as 5Pt-IWI-720. And the 1Pt/MAFO-IWI-300-5h and 1Pt/MAFO-IWI-800-5h samples are marked as Pt-IWI-300 and Pt-IWI-800. The Pt-IWI-800 SAC was tested for long-term stability, and the spent catalyst was marked as Pt-IWI-800-spent.

Preparation of Pt/$MgAl_2O_4$-CD samples

The 1Pt/$MgAl_2O_4$-CD-*T*-5h (marked as Pt/$MgAl_2O_4$-CD-*T*, *T* = 300, 600, 800°C) samples were prepared using the CD method and calcined in ambient air at *T* for 5 h with a heating rate of 2°C/min, similar to the preparation of the Pt/MAFO-CD samples.

Preparation of Pt/Fe_2O_3 samples

Fe_2O_3 support was prepared by calcining the iron(III) nitrate nonahydrate in ambient air at 700°C for 5 h with a heating rate of 2°C/min. And the single-atom Pt/Fe_2O_3 samples were prepared by using the CD method and IWI method, and calcined in ambient air at 800°C for 5 h, similar to our previous study [28]. The nominal weight loading of samples were 1 wt%. And the SACs are marked as Pt/Fe_2O_3-CD-800 and Pt/Fe_2O_3-IWI-800.

Characterization

X-ray diffraction (XRD) patterns were recorded on a PANalytical PW3040/60 X'Pert PRO diffractometer equipped with a Cu Kα radiation source (λ = 0.15432 nm), operated at 40 kV and 40 mA. A continuous mode was used for collecting data in the 2θ range of 15° to 80°.

The Brunauer-Emmett-Teller (BET) surface area was measured with a Micromeritics ASAP 2460 instrument using adsorption of N_2 at 77 K. All of the samples were degassed under vacuum at 300°C for 5 h before the adsorption measurements.

The actual loadings of Pt were determined by using ICP-OES on an Optima 7300DV instrument (PerkinElmer Instrument Corporation). All the samples were dissolved using aqua regia.

H_2 temperature programmed reduction (H_2-TPR) was performed on a TP-5080 multi-functional automatic adsorption instrument (Tianjin, Xianquan Industrial and Trading Co., Ltd.). Firstly, 50 mg of the Pt-CD-*T* sample or 15 mg of the other sample was loaded into a quartz reactor and pre-treated in air at 300°C for 1 h to remove adsorbed carbonates and hydrates before cooling down to room temperature. Then, the flowing gas was switched to a 5 vol% H_2/N_2 for 1 h at this temperature, and the sample was heated to 900°C with a heating rate of 10°C/min. The consumption of H_2 was calculated with the H_2 peak area and calibration curve of the 5 vol% H_2/N_2 standard gas.

High-angle annular dark-field scanning transmission electron microscopy (HAADF-STEM) images were obtained on a JEOL JEM-2100F operated at 200 kV. Aberration-corrected high-angle annular dark-field scanning transmission electron microscopy (AC HAADF-STEM) images were obtained on a JEOL JEM-ARM200F equipped with a CEOS probe corrector, with a guaranteed resolution of 0.08 nm. TEM specimens were prepared by depositing a suspension of the powdered sample on a lacey carbon-coated copper grid.

Infrared (IR) spectra were collected in a diffuse reflectance infrared Fourier transform spectroscopy (DRIFTS) mode using a Bruker EQUINOX 55 spectrometer, equipped with an MCT detector and operated at a resolution of 4 cm^{-1} for 64 scans. Before CO adsorption, the sample (~40 mg) was *in situ* pretreated in a flow (20 mL min^{-1}) of He at 300°C for 1 h in a DRIFTS cell (HC-500, Pike technologies). Then the sample was cooled to 50°C, hold for 60 min and background spectrum was collected. Subsequently, a mixture gas of 10 vol% CO/He (20 mL min^{-1}) was introduced into the reaction cell, and the spectra were collected with time until the saturation adsorption. Then switch the gas to He to purge the gaseous CO.

X-ray photoelectron spectroscopy (XPS) was measured on a Thermo Fisher ESCALAB 250Xi spectrometer equipped with an Al anode (Al Kα = 1486.6 eV), operated at 15 kV and 10.8 mA. The background pressure in the

analysis chamber was lower than 3×10^{-8} Pa, and the operating pressure was around 7.1×10^{-5} Pa. The survey and spectra were acquired at a pass-energy of 20 eV. Energy calibration was carried out using the C 1s peak of adventitious C at 284.8 eV.

X-ray absorption near edge structure (XANES) and extended X-ray absorption fine structure (EXAFS) spectra at the Pt L_{III} edge were recorded at the BL14W1, Shanghai Synchrotron Radiation Facility (SSRF), China. A Si (111) double-crystal monochromator was used for the energy selection. The energy was calibrated by Pt foil. Pt foil and PtO_2 were used as reference samples and measured in the transmission mode. Pt-CD-*T* samples were measured in fluorescence mode and 3Pt-CD-700 and 5Pt-IWI-720 were measured in the transmission mode. The Athena software package was used to analyze the data.

Density functional theory (DFT) calculations

The quantum chemical theoretical calculations were performed by using periodic DFT methods as implemented in the Vienna *ab-initio* simulation package (VASP) [32,33]. The core and valence electrons of all atoms were represented by the projector augmented wave (PAW) method [34] and the valence orbitals of Pt (5d, 6s), Al (3s, 3p), Fe (3d, 4s), Mg (3s, 3p) and O (2s, 2p) were described by plane-wave basis sets with cutoff energies of 400 eV. The exchange-correlation energies were calculated *via* the generalized gradient approximation (GGA) with the PBE functional [35]. Gaussian smearing method with a width of 0.05 eV was used. The Brillouin zone was sampled at the Γ-point. The convergence criteria for the energy and force were set to 10^{-5} eV and 0.02 eV $Å^{-1}$. To correct the strong electron-correlation properties of Fe 3d electrons in $MgAlFeO_4$, DFT+*U* calculations were performed with $U = 4.5$ eV for Fe.

$MgAl_2O_4$ spinel has a face-centered cubic (FCC) Bravais lattice, where the Mg^{2+} and Al^{3+} atoms occupy 1/8 tetrahedral positions and 1/2 octahedral positions of the FCC-like oxygen sub lattice, respectively. The half of Al^{3+} atoms are replaced by Fe^{3+} atoms, forming spinel $MgAlFeO_4$ structure. (111) surfaces cut from optimized cells are considered as supports. The $MgAl_2O_4$ (111) surface was modeled by p(2 × 2) supercells with the bottom eight layers ((-Mg-)\(-Al-)\(-Mg-)\(-O-O-O-)\(-O-) \(-Al-)\(-O-)\(-O-O-O-)) fixed. The vacuum gap was set as ~15 Å to avoid the interaction between the periodic images.

The formation energy of single-atom Pt_1 was applied to measure the stability of single-atom metal on the surface. Considering the oxidizing atmospheres, we calculated the $E_f(Pt_1) = E(Pt_1/MgAlFeO_4) - E(\text{support}) - \mu(Pt) - E(O_2)$, where $E(Pt_1/MgAlFeO_4)$, and $E(\text{support})$ are the calculated energy of $Pt_1/MgAlFeO_4$, and the corresponding support, respectively. And $\mu(Pt)$ represents the chemical potential of Pt in bulk Pt. The more negative formation energy of single-atom Pt_1 indicates the more stable SAC. Atomic charges were computed using the decomposition scheme proposed by Bader [36].

Catalytic reaction

N_2O decomposition was carried out at atmospheric pressure in a fixed-bed microreactor. 100 mg of catalyst diluted with 1 g of quartz sand (40–80 mesh) was loaded into a U-shaped quartz reactor. A k-type thermocouple in a thin quartz tube was inserted into the catalyst bed to measure the temperature. The feed gas containing 1000 ppm N_2O and balance Ar was passed through the reactor at 33.3 mL min^{-1}. Long-term stability was tested at 650°C for 100 h. The amounts of the N_2O in the inlet and outlet gas compositions were analyzed using a gas chromatograph (Echrom A91) equipped with Parapak Q packed column and a thermal conductivity detector using He as the carrier gas.

RESULTS

MAFO spinel was prepared by a solvothermal synthesis method. Small Pt NPs in size of ~2 nm were synthesized by a colloidal method and were deposited onto MAFO though a CD method. The schematic synthetic process is presented in Fig. S1 in Supplementary information (SI). The MAFO supported Pt samples were calcined at 300, 600 and 800°C, respectively, and denoted as Pt-CD-*T*, where *T* represents the calcination temperatures.

XRD characterization of the synthesized MAFO material shows it has pure spinel crystal phase (Fig. S2), indicating that Fe element is uniformly doped in the spinel. The surface area of the MAFO spinel is, as expected, much (about 10–20 times) higher than that of the Fe_2O_3 support (Table S1). After loading of Pt NPs, the spinel structure of all the Pt-CD samples remains unchanged (Fig. S2), suggesting that the thermal treatment does not induce phase transformation of the MAFO spinel. This result demonstrates that MAFO can be a promising robust support for preparing thermally stable catalysts. In addition, diffraction patterns of Pt species are not observed in all samples, indicating that Pt species are highly dispersed on the samples even after calcination at very high temperature of 600–800°C.

AC HAADF-STEM characterization was performed to reveal the Pt dispersion. Representative images are pre-

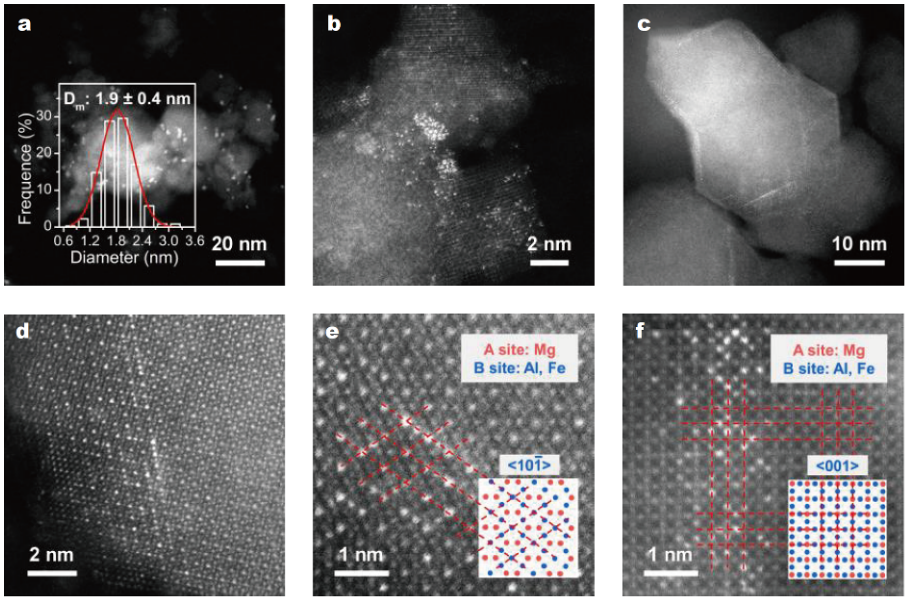

Figure 1 AC HAADF-STEM images of (a) Pt-CD-300, (b) Pt-CD-600, (c, d) Pt-CD-800 and the Pt-CD-800 sample in (e) <10$\bar{1}$> and (f) <001> directions (insets are patterns of A and B sites in AB_2O_4 spinel oxide).

sented in Fig. 1a–d and Fig. S3. On Pt-CD-300 sample, small and uniform Pt NPs with a mean size of 1.9 nm are clearly observed (Fig. 1a). The lattice spacing is 0.226 nm which corresponds to the Pt(111) plane (Fig. S3a, b), suggesting Pt NPs are crystalline. After calcination at 600°C, Pt NPs did not aggregate but dispersed into small clusters and single atoms (Fig. 1b and Fig. S3c, d). No large Pt NPs were observed in all regions, indicating that no sintering of Pt NPs occurred. Examination of Pt particles in different locations revealed that they virtually all consisted of randomly and loosely assembled single atoms, which were in contrast to the well-crystallized Pt NPs in the Pt-CD-300 sample. Increasing the calcination temperature to 800°C resulted in a full dispersion of Pt NPs into isolated Pt single atoms (Fig. 1c, d and Fig. S3e, f). Obviously, Pt NPs located on MAFO spinel were dispersed into single atoms upon high-temperature calcination in oxidizing atmosphere, which was consistent with our expectation. High-magnification images confirmed from different directions that Pt single atoms occupied exclusively the octahedral sites of the spinel structure and the position coincided exactly with the B sites (Fig. 1e, f).

The electron microscopy studies have unambiguously demonstrated that Pt NPs can be dispersed into single atoms upon high-temperature calcination on MAFO support. A control experiment can easily verify that the introduction of Fe plays a critical role in this dispersion process where Pt NPs on $MgAl_2O_4$ spinel sintered obviously after calcination at 600 and 800°C, as evidenced by XRD examination (Fig. S4). According to our previous work [28], we believe the critical role is related to the strong interaction between Pt and iron oxide. To confirm this, a series of investigations were further performed.

In situ DRIFTS of CO adsorption was studied on different Pt-CD-*T* samples. As shown in Fig. 2a, on Pt-CD-300 sample, three peaks centered at 2082, 2060 and 1820 cm^{-1} were clearly observed after the CO adsorption. The former two were attributed to the linearly adsorbed CO on Pt NPs at different locations and the latter was attributed to the bridged adsorption of CO on Pt NPs [37–39]. Differently, on Pt-CD-600/800 samples, no adsorption of CO was observed at all. Considering that no Pt loss was detected after calcination at high temperatures (Table S1), the possibility that the disappearance of CO adsorption might stem from volatilization of Pt can be excluded. Thus the result of no adsorption of CO should be related to the cationic nature of Pt [40] and may suggest a strong interaction between Pt and Fe.

The different interactions between Pt and Fe were further studied by H_2-TPR. As shown in Fig. 2b, for the Pt-CD-300 sample, the reduction of Pt species occurred at temperature below 150°C, similar to the reduction of Pt in the reported literature [41]. However, the reduction temperature of Pt increased with the calcination temperature (~200°C for Pt-CD-600 and ~300°C for Pt-CD-800 sample), suggesting that the metal-support interaction became stronger. Quantitative analysis of H_2 con-

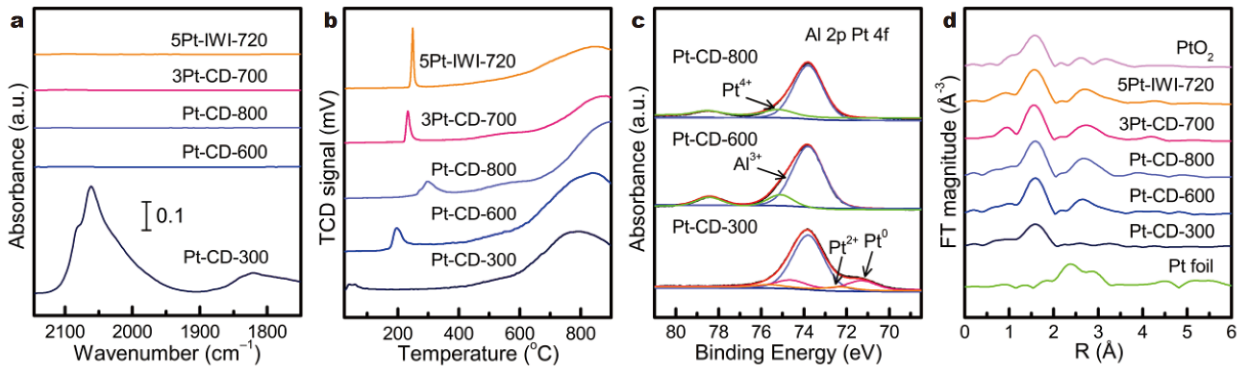

Figure 2 (a) CO-DRIFTS, (b) H_2-TPR profiles, (c) Al 2p-Pt 4f XPS, and (d) Fourier transform of EXAFS spectra at Pt L_{III} edge for the Pt/MAFO samples (without phase correction).

sumption amount (Table S2) revealed that the H_2 consumption on Pt-CD-300 was lower than the theoretical amount (assuming the reduction of PtO_2), but on Pt-CD-600 and 800, they were higher than the theoretical ones. The former owes to the low valence state of Pt colloidal NPs, while the latter indicates a reduction of the oxide that is closely contacted with Pt [42,43]. Considering the fact that Mg^{2+} and Al^{3+} in spinel are rather difficult to be reduced, we believe it is related to the reduction of Fe^{3+} species, evidencing the strong CMSI between Pt and FeO_x.

The valence states of Pt species were detected by XPS (Fig. 2c). By careful deconvolution of the overlapped peaks of Al 2p and Pt 4f, different Pt 4f peaks were obtained in the Pt-CD-*T* samples. For the Pt-CD-300 sample, two peaks located at about 71.3 and 72.3 eV were observed, representing $4f_{7/2}$ peaks of Pt^0 and Pt^{2+}, respectively [44,45], in good agreement with the H_2-TPR results. However, only Pt^{4+} ($4f_{7/2}$: 75.2 eV) existed in the 600 and 800°C calcined samples [46].

X-ray absorption spectroscopy (XAS) was measured to obtain more information on the valence and structure information of the Pt-CD-*T* samples. Fig. S5 shows the normalized XANES spectra of the samples by using Pt and PtO_2 as references. The white line intensities in the spectra reflect the oxidation state of Pt species [1,47]. For the Pt-CD-300 sample, the white line intensity exists between that of Pt foil and PtO_2, suggesting that the Pt species are positively charged. Correspondingly, the intensities of Pt-CD-600/800 samples are similar to that of PtO_2, indicating the Pt(IV) state in these two samples which agrees well with the XPS results.

EXAFS spectra is effective to reflect and characterize the local structure of measured element [3]. In the *r* range of 2.0–4.0 Å, the metallic Pt–Pt contribution were absent for the Pt-CD-800 samples, and a Pt–M (M = Mg, Al, Fe) or their mixture contribution was observed (Fig. 2d), unambiguously indicating the formation of Pt SAC. Detailed fitting parameters are shown in Table S3.

In order to investigate the thermal stability of the SACs, prolonged calcination of the Pt-CD sample at 800°C was performed for 10 and 24 h, respectively. The spinel structure was maintained and no diffraction peaks of Pt species were observed by XRD characterization (Fig. S6), indicating the SAC had excellent thermal stability upon long term calcination at such high temperatures.

Since the MAFO has much higher surface area compared with Fe_2O_3, a higher maximum Pt loading for maintaining the single-atom dispersion state can be expected. A detailed study revealed that the Pt SAC with a loading up to 3.1 wt% can be obtained (3Pt-CD-700, see Catalysts preparation section and Fig. 3a and Fig. S7). It is much higher (~3 times) than that on iron oxide (up to 1 wt%) [28], highlighting the advantages of using MAFO spinel as support.

IWI method is widely used in industrial supported metal catalyst production [48]. Compared with CD method, IWI is simpler and easier to implement. We therefore prepared a precursor catalyst by using IWI method for the following dispersion in order to check the generality of this NP dispersion process. It turns out that Pt NPs/clusters prepared by IWI with different loadings can be dispersed into single atoms (Fig. S8). Interestingly, even higher maximized Pt loading (up to 5 wt%) can be obtained by employing IWI method, which is in good agreement with our calculated theoretical maximum loading of dispersed Pt atoms over MAFO support (Details see SI). As shown in Fig. 3b and Fig. S9, high density of Pt single atoms was observed in the 5Pt-IWI-720 samples. The detailed data analysis was performed, i.e.,

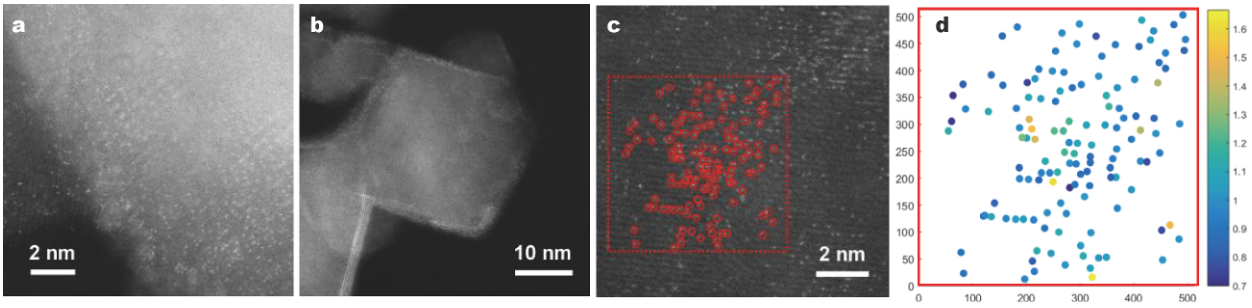

Figure 3 AC HAADF-STEM images of the (a) 3Pt-CD-700, (b, c) 5Pt-IWI-720. (d) Intensity analysis for the 5Pt-IWI-720 sample.

the signals of Pt atoms were extracted and normalized with the average HAADF-STEM signal (Fig. 3c, d). It can be seen that the intensity of most Pt atoms varies between 0.7 and 1.3, demonstrating that the Pt primarily exists in the form of single atoms [49].

Characterization experiments (XRD, CO-DRIFTS, H_2-TPR and XAS) were further performed on 3Pt-CD-700 and 5Pt-IWI-720 samples (Fig. 2, Figs S2 and S5). The results provide undoubted evidence for the formation of SACs and the existence of strong CMSI between Pt and MAFO spinel. The origins of the high thermal stability of Pt single atoms on MAFO support were further illustrated by DFT calculations. The (111) surfaces of $MgAlFeO_4$ and $MgAl_2O_4$ cut from optimized cells are considered as supports. Pt single atoms located at the octahedral sites by replacing one Al atom or Fe atom in $Pt_1/MgAlFeO_4$ (111) were considered and the optimized structures were shown in Fig. S10. In the $Pt_1/MgAlFeO_4$ (111) system, single-atom Pt_1 coordinated with three surface oxygen atoms and three subsurface oxygen atoms in an octahedron geometry with an average Pt–O length of 2.00 Å. The formation energy of single-atom Pt_1 was applied to measure its stability on the surface. The formation energy of Pt at the temperature of 1100 K at Fe and Al sites was −1.00 and −0.83 eV, respectively, much larger than that in $Pt_1/MgAl_2O_4$ (111) (−0.32 eV) (Fig. 4). The results suggest the introduction of Fe plays a critical role in stabilizing the Pt single atoms, well consistent with the experimental results (Fig. S4). The electronic structure of Pt_1 on $MgAlFeO_4$ (111) was also investigated. The Bader charge of Pt_1 was calculated to be +1.90 |e|, indicating the oxidation state of Pt_1 was +4, consistent with the XPS and XAS results. Hence, the strong CMSI between Pt_1 and $MgAlFeO_4$ was confirmed to be the origin of the high thermal stability.

With the highly stable SACs, we performed catalytic reactions to examine their performance. N_2O is a greenhouse gas with a warming potential about 310 times larger than that of CO_2. Meanwhile, it contributes to the depletion of stratospheric ozone. Among several N_2O elimination methods, catalytic decomposition seems to be the most promising one [50,51]. For this reaction, the O_2 desorption from catalyst surface has been regarded as the rate limit step [52]. SACs with high metal valence may

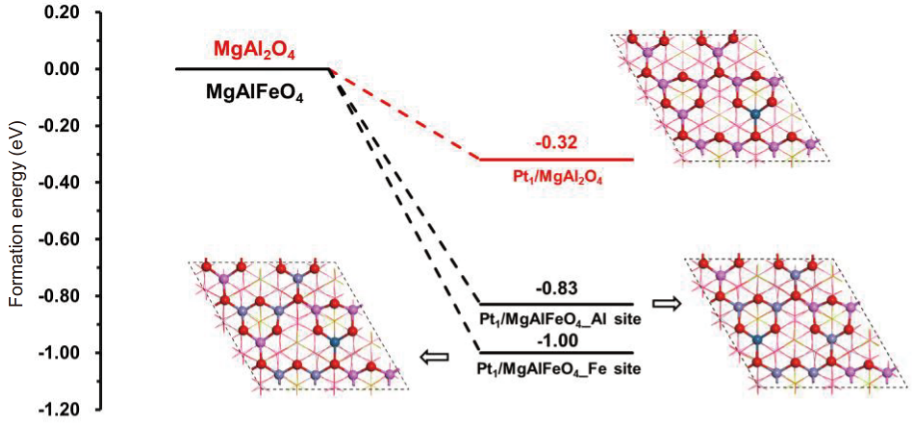

Figure 4 Structure and formation energy for the $Pt_1/MgAl_2O_4$ and $Pt_1/MgFeAlO_4$ at Al and Fe site at T = 1100 K. Color code: platinum (blue), oxygen (red), iron (purple), and aluminum (magenta).

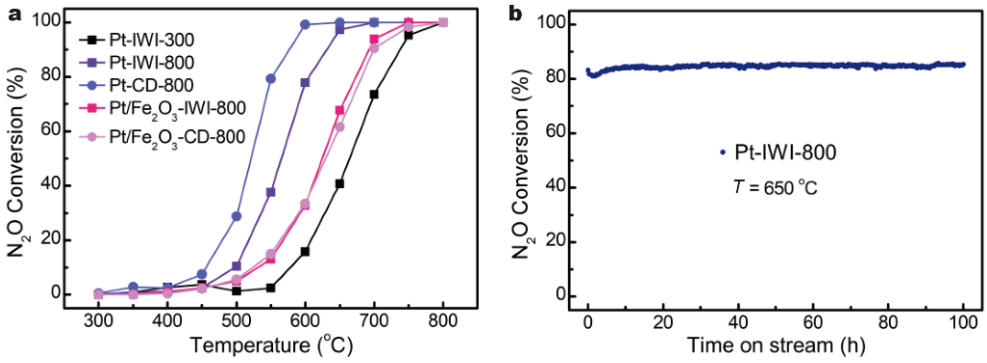

Figure 5 (a) N_2O conversion as a function of temperature for the Pt samples. Reaction conditions: 1000 ppm N_2O, and balance Ar. GHSV: 20,000 mL $g^{-1}_{cat.}$ h^{-1}. (b) The N_2O conversion as a function of reaction time on the Pt-IWI-800 catalyst tested at 650°C. Reaction conditions: 1000 ppm N_2O, and balance Ar. GHSV: 20,000 mL $g^{-1}_{cat.}$ h^{-1}.

have advantages over metallic state metal in facilitating the O_2 desorption. We therefore used N_2O decomposition as a probe reaction to evaluate the performance of MAFO supported Pt SACs and compared with their NP counterpart and Fe_2O_3-supported SACs. The Pt/Fe_2O_3-IWI/CD-800 SACs were prepared according to our previous study [28]. The metal loadings of all samples were set to be 1 wt%. The actual Pt loadings were similar to the nominal ones (Table S1). The Pt NP (~1 nm) of Pt-IWI-300 was confirmed by HAADF-STEM images (Fig. S11). N_2O conversion as a function of reaction temperature is presented in Fig. 5a. As expected, the Pt-IWI-800 SAC exhibited higher activity than the Pt-IWI-300 NP catalyst. Pt-CD-800 exhibited an even higher activity. Meanwhile, the MAFO supported SACs showed much higher activities compared with Fe_2O_3-supported SACs, irrespective the precursor prepared by IWI or CD method. To examine the SAC stability under reaction condition, Pt-IWI-800 sample was subjected to N_2O decomposition at 650°C, which showed that in a 100-hour run no deactivation was observed (Fig. 5b). The XRD and HAADF-STEM images of the post-reaction Pt-IWI-800 sample did not reveal the sintering of Pt single atoms after long-time reaction (Figs S12 and S13), evidencing the excellent high-temperature stability of the prepared SACs. These results demonstrate that the reducibility of the support is closely correlated with the stability of the metal SACs, as predicted previously [53,54].

CONCLUSIONS

In summary, on account of strong covalent metal-support interaction between Pt species and Fe-modified $MgAl_2O_4$ spinel ($MgAl_{1.2}Fe_{0.8}O_4$) support, high-loading and thermally stable Pt SACs can be fabricated from two Pt precursor catalysts prepared by IWI and CD methods. These Pt SACs exhibit better catalytic performance than either their NP counterpart or the Fe_2O_3-supported SACs for N_2O decomposition reaction. The strong covalent bonding between the support and the surface single atoms renders a class of high-temperature catalysts with well-defined single-atom active centers that might be modified for practical applications. This work demonstrates a general strategy for fabricating supported Pt SACs with high loading and excellent thermal stability by using Fe-doped materials as supports.

Received 1 February 2020; accepted 13 February 2020; published online 5 March 2020

1 Qiao B, Wang A, Yang X, *et al.* Single-atom catalysis of CO oxidation using Pt_1/FeO_x. Nat Chem, 2011, 3: 634–641
2 Yang XF, Wang A, Qiao B, *et al.* Single-atom catalysts: a new frontier in heterogeneous catalysis. Acc Chem Res, 2013, 46: 1740–1748
3 Liu J. Catalysis by supported single metal atoms. ACS Catal, 2017, 7: 34–59
4 Liu L, Corma A. Metal catalysts for heterogeneous catalysis: from single atoms to nanoclusters and nanoparticles. Chem Rev, 2018, 118: 4981–5079
5 Cui X, Li W, Ryabchuk P, *et al.* Bridging homogeneous and heterogeneous catalysis by heterogeneous single-metal-site catalysts. Nat Catal, 2018, 1: 385–397
6 Wang A, Li J, Zhang T. Heterogeneous single-atom catalysis. Nat Rev Chem, 2018, 2: 65–81
7 Zhang L, Zhou M, Wang A, *et al.* Selective hydrogenation over supported metal catalysts: from nanoparticles to single atoms. Chem Rev, 2020, 120: 683–733
8 Liu W, Zhang L, Liu X, *et al.* Discriminating catalytically active FeN_x species of atomically dispersed Fe–N–C catalyst for selective oxidation of the C–H bond. J Am Chem Soc, 2017, 139: 10790–10798
9 Nie L, Mei D, Xiong H, *et al.* Activation of surface lattice oxygen in single-atom Pt/CeO_2 for low-temperature CO oxidation. Science, 2017, 358: 1419–1423
10 Abdel-Mageed AM, Rungtaweevoranit B, Parlinska-Wojtan M, *et*

al. Highly active and stable single-atom Cu catalysts supported by a metal–organic framework. J Am Chem Soc, 2019, 141: 5201–5210
11 Wei H, Liu X, Wang A, *et al.* FeO_x-supported platinum single-atom and pseudo-single-atom catalysts for chemoselective hydrogenation of functionalized nitroarenes. Nat Commun, 2014, 5: 5634
12 Yan H, Zhao X, Guo N, *et al.* Atomic engineering of high-density isolated Co atoms on graphene with proximal-atom controlled reaction selectivity. Nat Commun, 2018, 9: 3197
13 Lin L, Yao S, Gao R, *et al.* A highly CO-tolerant atomically dispersed Pt catalyst for chemoselective hydrogenation. Nat Nanotechnol, 2019, 14: 354–361
14 Li T, Liu J, Song Y, *et al.* Photochemical solid-phase synthesis of platinum single atoms on nitrogen-doped carbon with high loading as bifunctional catalysts for hydrogen evolution and oxygen reduction reactions. ACS Catal, 2018, 8: 8450–8458
15 Qu Y, Chen B, Li Z, *et al.* Thermal emitting strategy to synthesize atomically dispersed Pt metal sites from bulk Pt metal. J Am Chem Soc, 2019, 141: 4505–4509
16 Zhao C, Wang Y, Li Z, *et al.* Solid-diffusion synthesis of single-atom catalysts directly from bulk metal for efficient CO_2 reduction. Joule, 2019, 3: 584–594
17 Zhang H, Wei J, Dong J, *et al.* Efficient visible-light-driven carbon dioxide reduction by a single-atom implanted metal-organic framework. Angew Chem Int Ed, 2016, 55: 1–6
18 Gao C, Chen S, Wang Y, *et al.* Heterogeneous single-atom catalyst for visible-light-driven high-turnover CO_2 reduction: the role of electron transfer. Adv Mater, 2018, 30: 1704624
19 Jones J, Xiong H, DeLaRiva AT, *et al.* Thermally stable single-atom platinum-on-ceria catalysts *via* atom trapping. Science, 2016, 353: 150–154
20 Zhang Z, Zhu Y, Asakura H, *et al.* Thermally stable single atom Pt/m-Al_2O_3 for selective hydrogenation and CO oxidation. Nat Commun, 2017, 8: 16100
21 Zhang L, Wang A, Wang W, *et al.* Co–N–C catalyst for C–C coupling reactions: on the catalytic performance and active sites. ACS Catal, 2015, 5: 6563–6572
22 Liu W, Zhang L, Yan W, *et al.* Single-atom dispersed Co–N–C catalyst: structure identification and performance for hydrogenative coupling of nitroarenes. Chem Sci, 2016, 7: 5758–5764
23 Peng Y, Lu B, Chen S. Carbon-supported single atom catalysts for electrochemical energy conversion and storage. Adv Mater, 2018, 30: 1801995
24 Yin P, Yao T, Wu Y, *et al.* Single cobalt atoms with precise N-coordination as superior oxygen reduction reaction catalysts. Angew Chem Int Ed, 2016, 55: 10800–10805
25 Qu Y, Li Z, Chen W, *et al.* Direct transformation of bulk copper into copper single sites *via* emitting and trapping of atoms. Nat Catal, 2018, 1: 781–786
26 Qiao B, Liang JX, Wang A, *et al.* Ultrastable single-atom gold catalysts with strong covalent metal-support interaction (CMSI). Nano Res, 2015, 8: 2913–2924
27 Qiao B, Liu J, Wang YG, *et al.* Highly efficient catalysis of preferential oxidation of CO in H_2-rich stream by gold single-atom catalysts. ACS Catal, 2015, 5: 6249–6254
28 Lang R, Xi W, Liu JC, *et al.* Non defect-stabilized thermally stable single-atom catalyst. Nat Commun, 2019, 10: 234
29 Li WZ, Kovarik L, Mei D, *et al.* Stable platinum nanoparticles on specific $MgAl_2O_4$ spinel facets at high temperatures in oxidizing atmospheres. Nat Commun, 2013, 4: 2481
30 Lu Y, Wang J, Yu L, *et al.* Identification of the active complex for CO oxidation over single-atom Ir-on-$MgAl_2O_4$ catalysts. Nat Catal, 2019, 2: 149–156
31 Wang Y, Ren J, Deng K, *et al.* Preparation of tractable platinum, rhodium, and ruthenium nanoclusters with small particle size in organic media. Chem Mater, 2000, 12: 1622–1627
32 Kresse G, Furthmüller J. Efficiency of *ab-initio* total energy calculations for metals and semiconductors using a plane-wave basis set. Comput Mater Sci, 1996, 6: 15–50
33 Kresse G, Furthmüller J. Efficient iterative schemes for *ab initio* total-energy calculations using a plane-wave basis set. Phys Rev B, 1996, 54: 11169–11186
34 Kresse G, Joubert D. From ultrasoft pseudopotentials to the projector augmented-wave method. Phys Rev B, 1999, 59: 1758–1775
35 Perdew JP, Burke K, Ernzerhof M. Generalized gradient approximation made simple. Phys Rev Lett, 1996, 77: 3865–3868
36 Bader RFW. A quantum theory of molecular structure and its applications. Chem Rev, 1991, 91: 893–928
37 Bazin P, Saur O, Lavalley JC, *et al.* FT-IR study of CO adsorption on Pt/CeO_2: characterisation and structural rearrangement of small Pt particles. Phys Chem Chem Phys, 2005, 7: 187
38 Jiang Z, Yang Y, Shangguan W, *et al.* Influence of support and metal precursor on the state and CO catalytic oxidation activity of platinum supported on TiO_2. J Phys Chem C, 2012, 116: 19396–19404
39 Ding K, Gulec A, Johnson AM, *et al.* Identification of active sites in CO oxidation and water-gas shift over supported Pt catalysts. Science, 2015, 350: 189–192
40 Liu L, Meira DM, Arenal R, *et al.* Determination of the evolution of heterogeneous single metal atoms and nanoclusters under reaction conditions: which are the working catalytic sites? ACS Catal, 2019, 9: 10626–10639
41 An N, Li S, Duchesne PN, *et al.* Size effects of platinum colloid particles on the structure and CO oxidation properties of supported Pt/Fe_2O_3 catalysts. J Phys Chem C, 2013, 117: 21254–21262
42 Lin J, Wang A, Qiao B, *et al.* Remarkable performance of Ir_1/FeO_x single-atom catalyst in water gas shift reaction. J Am Chem Soc, 2013, 135: 15314–15317
43 Lin J, Qiao B, Li N, *et al.* Little do more: a highly effective Pt_1/FeO_x single-atom catalyst for the reduction of NO by H_2. Chem Commun, 2015, 51: 7911–7914
44 Li Q, Wang K, Zhang S, *et al.* Effect of photocatalytic activity of CO oxidation on Pt/TiO_2 by strong interaction between Pt and TiO_2 under oxidizing atmosphere. J Mol Catal A-Chem, 2006, 258: 83–88
45 Şen F, Gökağaç G. Activity of carbon-supported platinum nanoparticles toward methanol oxidation reaction: role of metal precursor and a new surfactant, *tert*-octanethiol. J Phys Chem C, 2007, 111: 1467–1473
46 Zafeiratos S, Papakonstantinou G, Jacksic M, *et al.* The effect of Mo oxides and TiO_2 support on the chemisorption features of linearly adsorbed CO on Pt crystallites: an infrared and photoelectron spectroscopy study. J Catal, 2005, 232: 127–136
47 Bera P, Priolkar KR, Gayen A, *et al.* Ionic dispersion of Pt over CeO_2 by the combustion method: structural investigation by XRD, TEM, XPS, and EXAFS. Chem Mater, 2003, 15: 2049–2060
48 Munnik P, de Jongh PE, de Jong KP. Recent developments in the synthesis of supported catalysts. Chem Rev, 2015, 115: 6687–6718
49 Yu Z, Luo J, Shi B, *et al.* Embedding Ba monolayers and bilayers in boron carbide nanowires. Sci Rep, 2015, 5: 16960

50 Xue L, Zhang C, He H, *et al.* Catalytic decomposition of N_2O over CeO_2 promoted Co_3O_4 spinel catalyst. Appl Catal B-Environ, 2007, 75: 167–174
51 Asano K, Ohnishi C, Iwamoto S, *et al.* Potassium-doped Co_3O_4 catalyst for direct decomposition of N_2O. Appl Catal B-Environ, 2008, 78: 242–249
52 Kapteijn F, Rodriguez-Mirasol J, Moulijn JA. Heterogeneous catalytic decomposition of nitrous oxide. Appl Catal B-Environ, 1996, 9: 25–64
53 Liu JC, Wang YG, Li J. Toward rational design of oxide-supported single-atom catalysts: atomic dispersion of gold on ceria. J Am Chem Soc, 2017, 139: 6190–6199
54 Liu JC, Tang Y, Wang YG, *et al.* Theoretical understanding of the stability of single-atom catalysts. Natl Sci Rev, 2018, 5: 638–641

Acknowledgements This work was supported by the National Key Projects for Fundamental Research and Development of China (2016YFA0202801), the National Natural Science Foundation of China (21673226, 91645203 and 21590792), the "Transformational Technologies for Clean Energy and Demonstration", the Strategic Priority Research Program of the Chinese Academy of Sciences (XDA21040200 and XDB17000000). The calculations were performed by using supercomputers at Tsinghua National Laboratory for Information Science and Technology and the Computational Chemistry Laboratory of Department of Chemistry at Tsinghua University, which was supported by the Tsinghua Xuetang Talents Program. The synchrotron radiation experiment was performed at the BL14W1 at Shanghai Synchrotron Radiation Facility, China.

Author contributions Liu K synthesized the catalysts and performed most of the experiments, collected and analyzed the data. Tang Y and Li J performed DFT calculations and the theoretical analyses. Yu Z analyzed the STEM data. Ge B performed the aberration-corrected scanning transmission electron microscopy characterization. Ren G, Zhang J, Sun X and Chen Z did some experiments and characterizations. Ren Y and Liu X carried out the XAFS characterization. Liu K, Tang Y, Qiao B, Li WZ and Li J co-wrote the manuscript. Qiao B, Li W, Wang A and Li J designed the study and supervised the project. All authors contributed to the general discussion.

Conflict of interest The authors declare that they have no conflict of interest.

Supplementary information Supporting data are available in the online version of the paper.

Kaipeng Liu is currently a PhD candidate at Dalian Institute of Chemical Physics, Chinese Academy of Sciences. He received his BSc degree (majored in chemistry) from the College of Chemistry, Jilin University in 2014. His PhD research focuses on thermally stable single atom catalysis.

Yan Tang received her BSc degree from the School of Chemistry and Molecular Engineering, East China University of Science and Technology (ECUST) in 2014 and her PhD degree from Tsinghua University in 2019. Her PhD research focuses on the theoretical investigations on single atom catalysts (SACs).

Botao Qiao is currently a professor at Dalian Institute of Chemical Physics, Chinese Academy of Sciences. He received his PhD degree from Lanzhou Institute of Chemical Physics, Chinese Academy of Sciences in 2007, and then became a postdoctoral fellow in Dalian Institute of Chemical Physics where he has worked until present. He visited Arizona State University, USA, from 2012 to 2015. His research interests are focused on the design, synthesis and characterization of highly dispersed supported metal catalysts, especially on the subnano or single-atom catalysts.

Wei-Zhen Li received his PhD degree from Peking University in 2007. He did postdoctoral research at Tsinghua University from 2007 to 2009 and then at the Pacific Northwest National Laboratory (USA) from 2010 to 2014. He is now a full Professor at Dalian Institute of Chemical Physics, Chinese Academy of Sciences. His research focuses on heterogeneous catalysis, especially on designing of antisintering precious nanocatalysts for energy and environment related reactions under harsh reaction conditions.

Jun Li received his PhD degree from Fujian Institute of Research on the Structure of Matter, Chinese Academy of Sciences in 1992. He did postdoctoral research at the University of Siegen and the Ohio State University from 1994 to 1997. He worked as a research scientist at Ohio State University and senior research scientist at the Pacific Northwest National Laboratory from 1997 to 2009. He is now a full Professor at Tsinghua University. His research involves theoretical chemistry, heavy-element chemistry, and computational catalysis science.

高载量高温热稳定的$Pt_1/MgAl_{1.2}Fe_{0.8}O_4$单原子催化剂

刘凯鹏[1,2†], 汤妍[3†], 喻志阳[4], 葛炳辉[5], 任国庆[1,2], 任煜京[1,2], 苏杨[1], 张景才[1], 孙秀成[1,2], 陈志强[1], 刘晓艳[1], 乔波涛[1*], 李为臻[1*], 王爱琴[1], 李隽[3,6*]

摘要 近年来, 单原子催化剂(SACs)在非均相催化领域引起了广泛的关注. 然而, 制备高负载量和高热稳定的单原子催化剂(特别是在以氧化物作为载体的情况下)仍然是巨大的挑战. 在本工作中, 我们证明通过强共价金属-载体相互作用(CMSI), 使用铁改性的尖晶石作为载体, 可制得高负载和高温热稳定的Pt单原子催化剂. 对于N_2O分解反应, 此类单原子催化剂催化性能优于其相应的纳米催化剂和低表面积Fe_2O_3作为载体负载的Pt单原子催化剂. 本工作为在高温下制备高载量和热稳定的单原子催化剂提供了新的策略.

